SKIN FRICTION MEASUREMENTS ON A ROTOR IN HOVER

Alan J. Wadcock
Sterling Software, Palo Alto, CA

Gloria K. Yamauchi and David M. Driver
NASA Ames Research Center, Moffett Field, CA

Summary

The oil-film interferometric skin friction technique is described and applied to an isolated full-scale rotor in hover. This is the first time that this technique has been applied to a rotary wing. The chordwise component of skin friction is presented for both low and high thrust cases. The technique is shown to be capable of revealing the presence of natural transition, leading edge laminar separation followed by turbulent reattachment, and the presence of reversed flow.

Notation

c	local blade chord
C_f	local skin friction coefficient, τ / 0.50 ρ $(\Omega r)^2$
C_T	rotor thrust coeff., Thrust / ρ $(\Omega R)^2$ (πR^2)
h	oil film thickness
M_{tip}	tip Mach number
n_o	oil index of refraction
q	local dynamic pressure, $^1/_2\rho(\Omega r)^2$
r	radial location
R	rotor radius
Re	Reynolds number based on local blade chord and local rotational speed
s	distance along airfoil surface perpendicular to oil leading edge
t	time
T_r	recovery temperature
x	chordwise location
Δs_f	fringe spacing measured along airfoil surface, perpendicular to blade leading edge
λ	wavelength of illumination
μ_o	absolute viscosity of oil
ν_o	kinematic viscosity of oil
Θ	collective pitch angle measured at r/R = 0.75
Θ_i	incidence angle
Θ_r	refraction angle
ρ_o	oil density
τ	shear stress
Ω	rotor rotational rate, rad/sec

Presented at the American Helicopter Society Technical Specialists' Meeting for Rotorcraft Acoustics and Aerodynamics, October 28-30 1997, Williamsburg, VA.

Introduction

A recent review of the oil-film interferometry technique for the measurement of skin friction is provided by Driver[1]. This technique has been used in one form or another for the last twenty years[2,3]. The technique developed wide acceptance only after Monson *et al* [4] modified the technique in 1993 to make use of room lighting to visualize the interferometric pattern, and developed a simplified form of the oil-flow equation that only depends on the final state of the oil. As a result of these improvements the number of researchers in the field has grown rapidly[5-8].

The oil-film technique works on the principle that an oil film will thin at a rate that is proportional to the applied shear. The technique requires a knowledge of the "air on" time history of the dynamic pressure and blade temperature, knowledge of the properties of the oil, and measurement of the final oil-thickness distribution. The oil-thickness distribution is determined from the pattern produced in the oil film by interference between light reflected from the model surface and that relected from the oil-air interface, as shown in Figure 1. The fringes observed in each oil film are contours of constant oil thickness, and fringe number can be related to the oil depth, h.

The oil-film technique was originally developed for use with fixed-wing wind-tunnel models. As long as the flow conditions are steady, as in hover, this technique can be applied to rotary wings also. The current measurements were acquired during the March 1997 hover test of a full-scale XV-15 tiltrotor in the 80- by 120-Ft Wind Tunnel at NASA Ames and represent the first time this technique has been applied to a rotary wing.

Theory

Following Monson *et al* [4] it can be shown that the fringe spacing is proportional to the skin friction coefficient. Starting with the differential form of the oil flow equation from 1-D hydraulics

$$\frac{dh}{dt} = -\frac{1}{2\mu_0}\frac{d}{dx}\left(\tau h^2\right) \qquad (1)$$

where h is the oil thickness, μ_0 is the oil viscosity and τ the shear stress.

Using separation of variables, it can be shown that

$$h = \frac{\mu_0 x}{\tau t}$$

An intermediate form of the equation is obtained by integrating Eq. 1 with respect to x,

$$\tau/(\mu_0 x) = -\frac{1}{h^2}\frac{dh}{dt} \qquad (2)$$

where x is the distance downstream from the leading edge of the oil and h is the thickness of the oil at location x. Hence, substituting for $\tau = q_\infty C_f$ and integrating with respect to time we obtain

$$\int_0^t (q_\infty C_f)/(\mu_0 x)dt = -\int_0^t \left(\frac{1}{h^2}\frac{dh}{dt}\right)dt \qquad (3)$$

Assuming C_f is constant during the run, we obtain

$$(C_f/x)\int_0^t \frac{q_\infty}{\mu_0}dt = \left[\frac{1}{h}\right]_{h_i}^{h} \qquad (4)$$

The lower limit on (1/h) is assumed to be negligibly small (compared to the upper limit) as the initial oil thickness is usually large compared to the final oil thickness. Rearranging, we obtain

$$C_f = \frac{x}{h}\Big/\int_0^t \frac{q_\infty}{\mu_0}dt \qquad (5)$$

This equation is presented in Monson *et al* [4]. Note that the initial oil film thickness is assumed infinite. Although not infinite in practice, the initial oil film thickness is large --- on the order of 100λ, making this a reasonable assumption. Finally, we obtain

$$C_{f_s} = \left(\frac{2n_0 \cos\Theta_r \Delta s_f}{\lambda}\right)\Big/\int_0^{t_{run}} \frac{q_\infty(t)}{\mu_0(t)}dt \qquad (6)$$

where the suffix "s" has been added to emphasize that the current skin friction measurements are made in a direction perpendicular to the blade leading-edge with fringe-spacing Δs_f along the curved surface of the airfoil. Eq. 6 indicates that skin friction is directly proportional to fringe spacing. The first grouping on the right hand side of the equation is the reciprocal of the oil-film slope and the integral contains the oil viscosity and the free-stream dynamic pressure, both of which may vary during the run.

The shear stress referred to in this equation is the component of shear stress that is perpendicular to the leading edge of the oil. The component of shear stress that is parallel to the oil-film leading edge does not influence the development of the oil film in the perpendicular direction.

It is useful at this point to consider the effect of centrifugal force on the oil film development. At the blade tip, $\Omega^2 R$ is approximately 1500 g ----- many times the gravitational force. The important parameter, however, is the ratio of the aerodynamic force to the centrifugal force acting on the oil film. This ratio is easily shown to be

$$\frac{aerodynamic}{centrifugal} = C_f\left(\frac{\rho_\infty}{\rho_0}\right)\left(\frac{r}{h}\right) \qquad (7)$$

This equation clearly indicates that centrifugal forces will be least important at the blade tip (since aerodynamic forces vary as V^2 yet centrifugal forces vary as V^2/r) and become more important close to the blade root. During the initial spin-up transient, at which time the oil film thickness h is a maximum, centrifugal forces will be most significant. The air density is small compared to the oil density, but the radial location is large (measured in meters) compared to the oil film thickness (measured in microns) and so the centrifugal force can be made negligible if the oil is allowed to thin sufficiently. For a density ratio of 800 between oil and air and a typical C_f of 0.005, at 0.94R the ratio of aerodynamic force to centrifugal force has the value of 228 at the location of the first dark fringe, 76 at the second, 46 at the third, and so on. At the most inboard radial station of 0.17R the corresponding ratios are 41, 14 and 8.

Experimental Installation

Figure 2 shows the full-scale XV-15 rotor system mounted on the Rotor Test Apparatus (RTA) test stand in the test section of the NASA Ames 80- by 120-Ft Wind Tunnel. This is an open-circuit wind tunnel with a rectangular test section that is 80-ft high, 120-ft wide and 193-ft long. The RTA is a special-purpose test stand developed for operating rotors in the 40- by 80-Ft and 80- by 120-Ft Wind Tunnels at NASA Ames. The RTA was mounted in the wind tunnel on a three-strut support system --- two main struts and one tail strut --- placing the rotor hub approximately 31 ft above the test section floor. Additional details of the RTA can be found in Reference 9.

The XV-15 rotor system consists of three highly twisted, square tip metal blades of radius 12.5 ft (Table

1). Figure 3(a) shows the variation of blade chord with radial station. The blade has a constant chord of 14 in for r/R > 0.25. Figure 3(b) shows the blade twist distribution and Figure 3(c) the blade section at each of the radial stations chosen for the skin friction measurements.

Procedure

The test surface must be prepared so that it is optically smooth and partially reflective. To accomplish this, thin sheets of MonoKote[10] (Mylar with black pigment and adhesive backing) were applied to a single blade at the radial stations of interest. This material is 0.003-in thick and is available in sheets of size 36-in long by 5-in wide. The radial stations chosen were 0.17R, 0.28R, 0.50R, 0.72R, 0.83R and 0.94R. The quoted radial station refers to the center location of each Mylar strip. Before applying Mylar to the chosen blade, the blade was thoroughly cleaned --- first with a glass-cleaning detergent and then with alcohol. A single piece of Mylar was wrapped around the blade at each of the selected radial stations, starting at the trailing edge on the blade upper surface. Instrumentation wires, covered with epoxy, run the length of the blade at x/c $\approx$ 0.75, and the unbroken Mylar film was laid over the top of the raised areas that accommodate these wires. The instrumentation strip presents only a minimal disturbance to the flow and is not believed to significantly affect the skin friction measurements. The raised area of epoxy that runs from root to tip on the blade is about 1 to 1.5 in wide and 0.007 in thick at both edges but is somewhat thicker in the center of the strip where the wires are located. The cross-sectional shape of this raised area is approximately triangular, the maximum thickness being located immediately above the instrumentation wires.

The Mylar was cleaned with both detergent and alcohol prior to applying oil before each run. The oil viscosity chosen for each Mylar station was based on the dynamic pressure at that radial location and the run duration, as shown in Table 2. Prior to each run approximately 20 to 25 oil lines were applied parallel to the blade leading edge on each Mylar film using a rubber applicator. Each oil line was about 0.5-in long. In addition, several oil lines were applied perpendicular to the blade leading edge in the hope of determining the radial component of shear stress. A staggered diagonal pattern of oil lines was used to minimize the interference between adjacent oil films caused by oil that is spun radially outwards under the action of centrifugal force during the initial moments of rotor spin-up. A full-size oil-application template for each radial station was used in order to achieve a desired oil-film pattern, and Figure 4 shows the templates in use. The corresponding template is shown positioned adjacent to each Mylar film.

High viscosity oil is used at the blade tip and low viscosity oil at the blade root because of the large variation in dynamic pressure with radial station. Recall that the blade is highly twisted as shown in Figure 3(b) and Figure 4. To reduce gravitational effects on the applied oil lines prior to rotor spin-up, oil lines were applied starting at the outermost radial station and working progressively inboard. Any time interval between oil application and rotor spin-up that results in gravitational oil flow can alter the shape of the oil lines and make the interpretation of the resulting fringe patterns more difficult. In addition to minimizing gravitational effects on the oil prior to rotor spin-up, any delay should be avoided in order to minimize dust deposition on either the oil or the Mylar. The collective pitch was set immediately after the oil had been applied and was not changed for the duration of the run. The rotor was started and rpm was increased rapidly until the nominal 589 rpm was achieved, at which point the rpm was adjusted to deliver the desired tip Mach number of 0.690. Figure 5 shows a typical time history for rotor rpm. A time "on condition" of 15 minutes was chosen in order to deliver fringe spacings of the desired size. During this time "on condition" rotor balance data were acquired spaced about 1 minute apart. The rpm time history was recorded in order to account for the initial "spin-up" and final "spin-down" transients as indicated by the time dependent terms in Eq. 6.

After completion of the run, there is less urgency to reach the model and photograph the oil film patterns as the oil films are so thin that they will not change measurably with time due to gravity. Figure 6 illustrates the procedure used to photograph the oil film patterns. An adhesive-backed tape measure was placed adjacent to each Mylar film to provide scale in each photograph. In order to document the complete blade chord at each radial station a large distributed light source is needed. This was created using a semi-circular structure placed above the Mylar film and a pair of Dyna-Lite studio lights located on the floor, either side of the blade. Each Dyna-Lite is equipped with a convenient 250-Watt continuous light source that was used for focussing the camera. The high contrast of the tape measure graduations (compared to the fringe patterns) led to the use of the tape measure as an aid in camera focussing. Each Dyna-Lite is also equipped with a 500-J Xenon flash lamp, where the flash source was chosen for image acquisition in order to minimize effects of camera motion.

A Kodak DCS 460 digital camera with a variable 35 - 80 mm zoom lens and a notch filter centered on 551.8 nm with 18.8 nm FWHM and maximum

transmission of 65% was used to photograph the fringe patterns. Shutter speed was 1/125 sec at F/11 for the global images and F/8 for the close-ups. The camera was mounted on a tripod for stability, and the tripod straddled the Mylar at the radial station of interest. Each digital image is 3060 x 2036 pixels in size, each pixel being 24 bits deep (8 bits for each of R, G and B). Each of these color images was transferred to CD-ROM for permanent storage. During this storage process corresponding greyscale images were also archived in order to simplify data handling during post-processing.

A Nikon 35mm camera was successfully used to photograph the fringe patterns in a few early runs. Black and white TMAX 100 ASA or TMAX 400 ASA film was used with the same 35 - 80 mm zoom lens. The camera was equipped with a 500 to 570 nm notch filter, illumination being provided by two Mercury fluorescent flood lamps (strong emission at 546nm) or two Xenon flash lamps and the same umbrella-shaped reflector used throughout the test. The digital camera was ultimately selected over the 35mm camera to avoid the turnaround time associated with developing and printing the film.

The fringe patterns were analysed using *Image*, a public domain image-processing program developed by the National Institutes of Health. In general, 3 to 5 dark fringes were visible in each fringe pattern. The center of each dark fringe in a given fringe pattern was identified, and the pixel coordinates noted. Each pair of fringes provides a measurement of fringe spacing to be used in Eq. 6. Each oil pattern therefore provides more than one measurement of skin friction, the number of such measurements depending on the number of visible fringe-pairs. Image scale was provided by the tape measure mounted adjacent to the Mylar film. Pixel locations corresponding to each 1/2-in graduation on the tape were curve fit to a polynomial function of chordwise location on the blade in order to reduce the uncertainty in any local measurement of scale.

Results and Discussion

The wind tunnel test boundary was limited to the 1-g flight envelope of the XV-15 aircraft. At the design tip Mach number of 0.690 the rotor system was thrust limited and conditions for rotor stall were not achievable. At reduced rpm ($M_{tip} = 0.560$) a collective pitch of almost 17 deg was achievable before becoming torque limited. A complete set of skin friction data was successfully acquired at reduced rpm for collective angles from 3 deg to 17 deg and rotor stall was achieved without exceeding any structural limitations. No investigation of blade-to-blade differences was considered. Only the upper surface of the chosen blade was used for this study.

The current paper presents results from two hover test conditions only, both at the design tip Mach number of 0.690. The first is a low thrust condition at a collective pitch of 3 deg with $C_T = 0.0035$ and the second condition is at a collective pitch of 10 deg (corresponding to 1-g hover) with $C_T = 0.0093$ (see Table 2).

At each radial station, a "global" photograph of the oil-film patterns was taken in order to document the full blade chord. The initial intent was to use the global photographs for information purposes only --- to give a "global perspective" to what was happening over the full blade chord. In addition, three or four close-up photographs were acquired at each radial location. The close-up images were to be used for data reduction and the global images were available in case there were any problems with the close-up images. The global images provided by the high resolution digital camera, however, were more than adequate for data processing. Having the full blade chord in a single image also simplified the data analysis. The only data presented in the current paper comes from the global images.

A typical global fringe pattern from the low thrust condition at radial station r = 0.721R is shown in Figure 7. Note the tape measure identifying the radial station adjacent to the Mylar film. This tape measure is used to define image scale. Also note the epoxy strip that contains the instrumentation wires crossing beneath the Mylar film between 3.25 and 4.25 in from the blade trailing edge. The dark circular patch in the center of the Mylar film is the image of the cut-out in the distributed source through which the camera is viewing the fringe pattern. No information is available inside this area. The fringe patterns clearly show a fringe spacing that decreases with increasing distance from the blade leading edge for $0.0 < x/c < 0.40$, followed by a discontinuous increase in fringe spacing at about 40% chord followed by another decrease in fringe spacing for $0.40 < x/c < 1.00$. Since fringe spacing is proportional to shear stress, it is evident that the boundary layer is initially laminar and undergoes transition close to the 40% chord location to a turbulent boundary layer with higher associated shear stress.

A global fringe pattern from the high thrust (1-g hover) condition at radial station r = 0.28R is shown in Figure 8. This radial station appears to show an orderly transition from laminar to turbulent flow at about 15% blade chord followed by a region of reversed-flow at about 75% blade chord. The figure shows a close-up at x/c = 0.75 revealing fringing on the trailing-edge of oil that was centrifuged radially outwards during the initial rotor spin-up, indicating that this is the effective leading-edge of the oil film and that flow direction on the blade surface has reversed. The flow is believed to be predominantly radial at this location with a small

component of shear in the minus x direction. Beyond x/c = 0.80 no chordwise fringes are evident, presumably because the chordwise component of shear is very close to zero. The flow is believed to be highly three-dimensional in this vicinity with the shear vector pointing radially outwards. Figure 8 also illustrates the use of chordwise oil lines in an attempt to measure the radial component of skin friction. Fringe spacing in the radial direction is clearly non-linear. Tanner and Blows[2] predict a parabolic variation of oil film thickness with radial position for an oil film under pure rotation with no shear. Determination of the radial component of skin friction using this technique is being investigated.

Table 2 lists the mean M_{tip}, ambient temperature, effective run duration and nominal oil viscosity used at each radial station for both test conditions. The recovery temperature is estimated at each radial station from the tabulated M_{tip} permitting a more accurate estimate for both oil viscosity and oil density. Oil viscosity was computed from an "in-house" calibration and the estimated oil temperature. Oil temperature was estimated using a recovery factor of 0.87 (a compromise between the value of 0.85 appropriate for laminar boundary layers and 0.89 for turbulent), the local radius, and the mean M_{tip} during the run. Oil temperature was assumed to be constant during the run. The oil viscosity is moderately sensitive to temperature. Table 2 lists estimated blade temperature as a function of radial location. Note that the temperature at the blade tip was approximately 20 deg C greater than at the blade root. The uncertainty in the oil temperature could be reduced by using values for the recovery factor that are appropriate to the local boundary layer state (either laminar or turbulent). This would change the recovery factor by +/- 2.3% from the compromise value of 0.87, changing blade temperature by at most 0.5 deg C and viscosity by 1%. Values of shear stress were non-dimensionalized using the dynamic pressure based on rpm and the mean radial location of each Mylar film. This non-dimensionalization is expected to produce a "spread" of +/- 4% in C_f at 0.94R rising to +/-20% at 0.17R due to the variation in dynamic pressure from one side of the Mylar film to the other. In addition, calculation of skin friction also requires knowledge of the $\cos\Theta_T$ term in Eq. 6. The current paper assumes this term is equal to unity. Strictly speaking, this is only true when the camera is perpendicular to the local blade surface. The maximum error is estimated to be of order 5% and will be largest at the blade leading and trailing edges.

Figure 9 presents measurements of the chordwise component of skin friction measured along the blade surface for a collective pitch of 3 deg. At each radial station the chordwise location where the instrumentation wiring passes beneath the Mylar is identified. At the most inboard radial station, 0.17R, the boundary layer is initially laminar as the flow comes around the blade leading edge. The skin friction decreases with increasing x/c until about 35% chord at which point the boundary layer becomes turbulent. The skin friction increases very rapidly in the transition region, but decreases thereafter with increasing x/c. No chordwise fringes were evident in the last 10% of the blade chord, presumably due to zero chordwise shear. Radial station 0.28R shows a similar behaviour with evidence of transition at about 35% chord. Radial station 0.50R shows increased scatter caused by the appearance of a turbulent wedge originating in the middle of the Mylar film very close to the blade leading edge. The turbulent wedge subtended an angle of about 19 deg, in good agreement with the value of 18 deg quoted by Kuethe and Schetzer[11]. This turbulent wedge was apparently caused by the Mylar film starting to separate from its adhesive backing and form "bubbles" beneath the Mylar. All subsequent downstream measurements of skin friction reflect their upstream history to a certain degree and so more scatter is expected depending on the lateral location of individual measurements on the Mylar. Radial station 0.72R has already been described with reference to Figure 7. Radial station 0.83R has no data for $0.35 < x/c < 0.55$ due to one oil pattern being of extremely poor quality and the other being obscured by the dark spot in the photograph caused by the image of the camera lens. Unfortunately, boundary layer transition occurs in this region leaving us unable to specify the precise chordwise location at which this occurred. Measurements at radial station 0.94R indicate transition at about 50% chord. Much of the increased scatter observed at the inboard stations is due to the use of the dynamic pressure at the middle of each Mylar strip to non-dimensionalize the shear measurements, as discussed earlier. Such scatter should not be interpreted as uncertainty in the C_f measurements but simply represents the variation in dynamic pressure across the width of each Mylar strip.

Figure 10 presents similar measurements for a collective pitch of 10 deg corresponding to 1-g hover. The boundary layer is believed to be turbulent at the most upstream measurement location for station 0.17R. Station 0.28R has already been described in detail with reference to Figure 8. At 0.50R, a laminar leading edge bubble was observed followed by turbulent reattachment. The upstream and downstream edges of this bubble were assigned zero shear stress in the figure. Downstream of x/c = 75% no chordwise fringes were observed, and once again this is attributed to zero shear in the chordwise direction. At 0.72R the boundary layer is initially laminar and undergoes transition upstream of x/c = 15%. Thereafter the turbulent skin friction decreases smoothly with increasing x/c and the boundary layer is still quite healthy at the blade trailing edge. At 0.83R transition occurs in the vicinity of the quarter

chord location, but at 0.94R no obvious transition is evident. As the Reynolds number at the blade tip is almost 5 million, the boundary layer is most likely turbulent from the blade leading-edge.

Measurements of transition location inferred from Figures 9 and 10 are presented in Figure 11. The "uncertainty" bars represent the streamwise extent between the most downstream laminar point and the most upstream fully turbulent point. Transition is defined as the mid-point of this range in x/c. As expected at high thrust, transition was found to occur close to the blade leading edge, although somewhat irregularly with radial location. At low thrust, the blade has extensive regions of laminar flow and transition varies smoothly from x/c = 35% at the blade root to x/c > 50% at the blade tip.

Conclusions

This paper describes the first application of oil-film interferometry to the measurement of skin friction on a rotary wing. The technique was applied to a full-scale XV-15 tilt rotor in hover for both low and high thrust conditions at design tip Mach number. The technique is shown to be capable of revealing laminar leading-edge bubbles, transition and reverse-flow.

Extensive regions of laminar flow exist at 3 deg collective. The low thrust dataset should prove useful in validating transition prediction. Transition is shown to move close to the blade leading edge at 10 degrees collective. The high thrust case, corresponding to 1-g hover, is surprising in that reverse-flow is shown to exist over a significant extent of the chord at the 28% radial station. The high thrust dataset should prove useful for hover code validation.

The current measurements described in this paper are limited to the chordwise component of skin friction. Measurement of the radial component of skin friction will be addressed in the very near future. The goal is to provide shear stress in both magnitude and direction.

Acknowledgements

The authors would like to thank J. T. Heineck for assisting with initial testing in late 1996, Robert Kennelly for many informative discussions and the loan of the notch filter, and most of all Tom Reddy for his enthusiastic assistance with image acquisition throughout the test.

References

1. Driver, D. M., "Application of oil-film interferometry skin friction to large wind tunnels," AGARD Conference Proceedings CP-601, Paper No. 25, RTO/AGARD/FDP 81st Symposium on Advanced Aerodynamic Measurement Technology, Seattle, Washington, September, 1997.

2. Tanner, L. H. and Blows, L. G., "A study of the motion of oil films on surfaces in air flows, with application to the measurement of skin friction," *Journal of Physics* E: Scientific Instrumentation, Volume 9, No. 3, pp. 194-202, March 1976.

3. Monson, D. J., "A nonintrusive laser interferometer method for measurement of skin friction," *Experiments in Fluids*, Volume 1, No. 1, pp.15-22, 1983.

4. Monson, D. J., Mateer, G. G. and Menter, F. R., "Boundary-layer transition and global skin friction measurement with an oil-fringe imaging technique," SAE Paper 932550, September 1993.

5. Kennelly, R. A. Jr., Westphal, R. V., Mateer, G. G. and Seelen, J., "Surface oil film interferometry on a swept wing model in supersonic flow," Proceedings of the 7th International Symposium on Flow Visualization, Seattle, Washington, September 1995.

6. Naughton, J. W. and Brown, J. L., "Surface interferometric skin-friction measurement technique," AIAA Paper 96-2183, July 1996.

7. Garrison, T. J. and Ackman, M., "Development of a global interferometer skin-friction meter," AIAA Paper 96-1968, July 1996.

8. Zilliac, G. G., "Further developments of the fringe imaging skin friction technique," NASA TM 110425, December 1996.

9. Light, Jeffrey S., "Results from an XV-15 rotor test in the National Full-Scale Aerodynamics Complex," National Forum of the American Helicopter Society, Virginia Beach, Virginia, April 1997.

10. MonoKote, Top Flite Corporation.

11. Kuethe, A. M. and Schetzer, J. D., *Foundations of Aerodynamics*, p. 287, 2nd edition, Wiley and Sons, 1959.

Table 1. XV-15 rotor characteristics

Number of blades, N_b	3
Rotor radius	12.5 ft
Blade chord at tip	14 in
Rotor solidity, σ	0.089
Blade twist	-41 deg (non-linear)
Hub pre-cone angle	1.5 deg
Rotor airfoils	NACA 64-series

Table 2. XV-15 hover test conditions

Table (2a). RUN 80; collective pitch = 10.04 degrees.

Ω = 587.37 rpm, M_{tip} = 0.6902, Re_{tip} = 4.925 million, C_T = 0.00927
$T_{ambient}$ = 13.76 °C, effective time "on condition" = 17.950 mins.

r/R	0.170	0.280	0.500	0.721	0.830	0.940
nominal ν_o, cS	500	500	1000	1000	2000	2000
n_o	1.4033	1.4033	1.4035	1.4035	1.4035	1.4035
T_r, °C	14.44	15.62	19.70	26.12	30.14	34.77
ν_o, cS	596.4	581.7	1053	926	1588	1456
ρ_o, kg/m^3	981.8	980.7	976.9	970.9	967.1	962.8

Table (2b). RUN 81; collective pitch = 2.92 degrees.

Ω = 585.91 rpm, M_{tip} = 0.6897, Re_{tip} = 4.951 million, C_T = 0.00347
$T_{ambient}$ = 12.76 °C, effective time "on condition" = 17.475 mins.

r/R	0.170	0.280	0.500	0.721	0.830	0.940
nominal ν_o, cS	500	500	1000	1000	2000	2000
n_o	1.4033	1.4033	1.4035	1.4035	1.4035	1.4035
T_r, °C	13.44	14.61	18.67	25.06	29.06	33.67
ν_o, cS	609.2	594.3	1075.3	945.4	1621.5	1486.0
ρ_o, kg/m^3	982.7	981.6	977.8	971.8	968.1	963.8

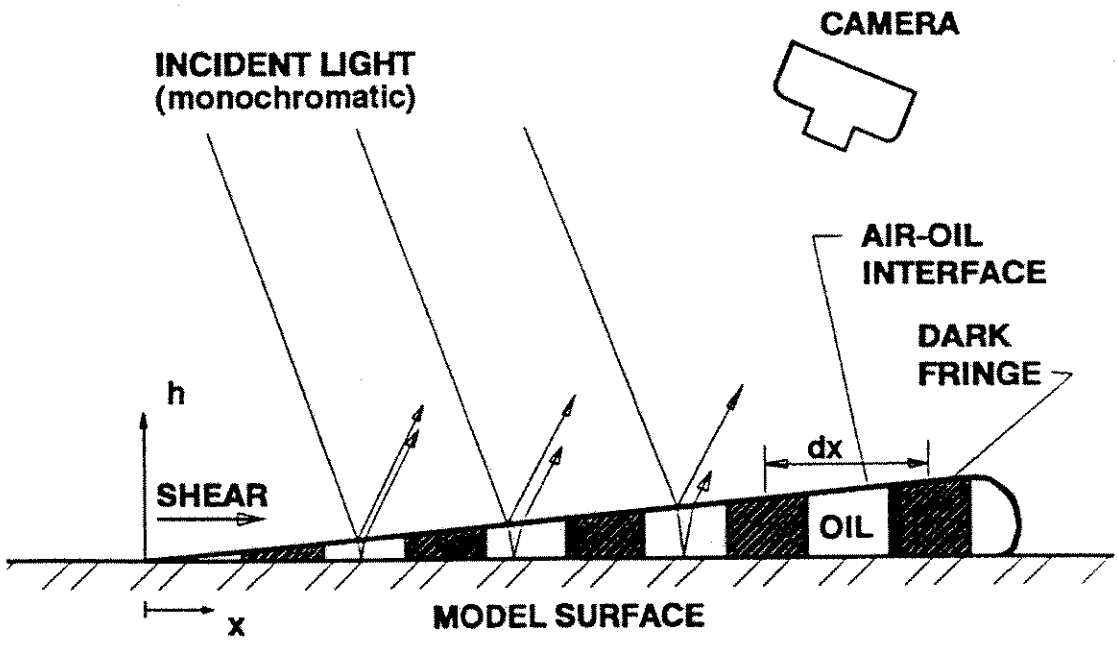

Figure 1. Schematic of oil-film interference pattern.

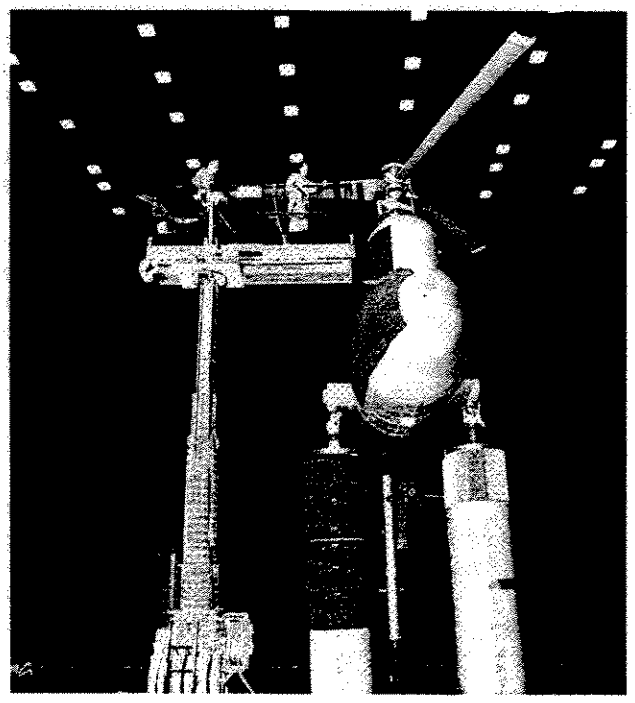

Figure 2. XV15/RTA test installation in the 80- by 120-foot wind tunnel.

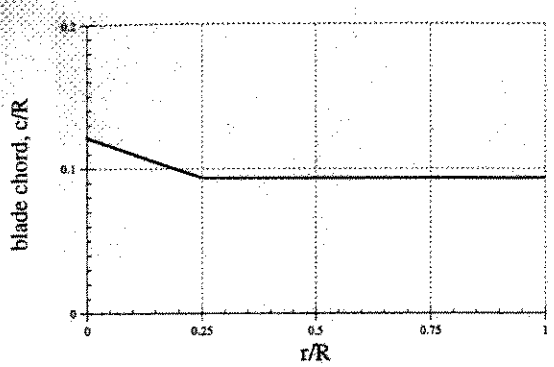

Figure 3(a). Blade chord distribution.

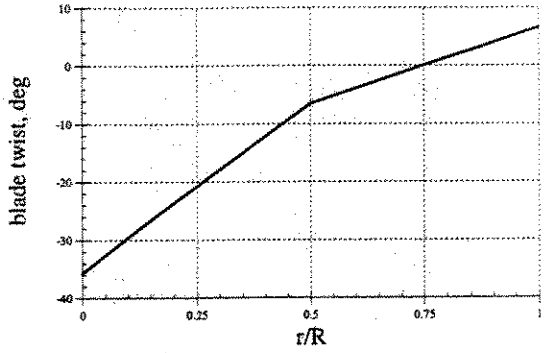

Figure 3(b). Blade twist distribution.

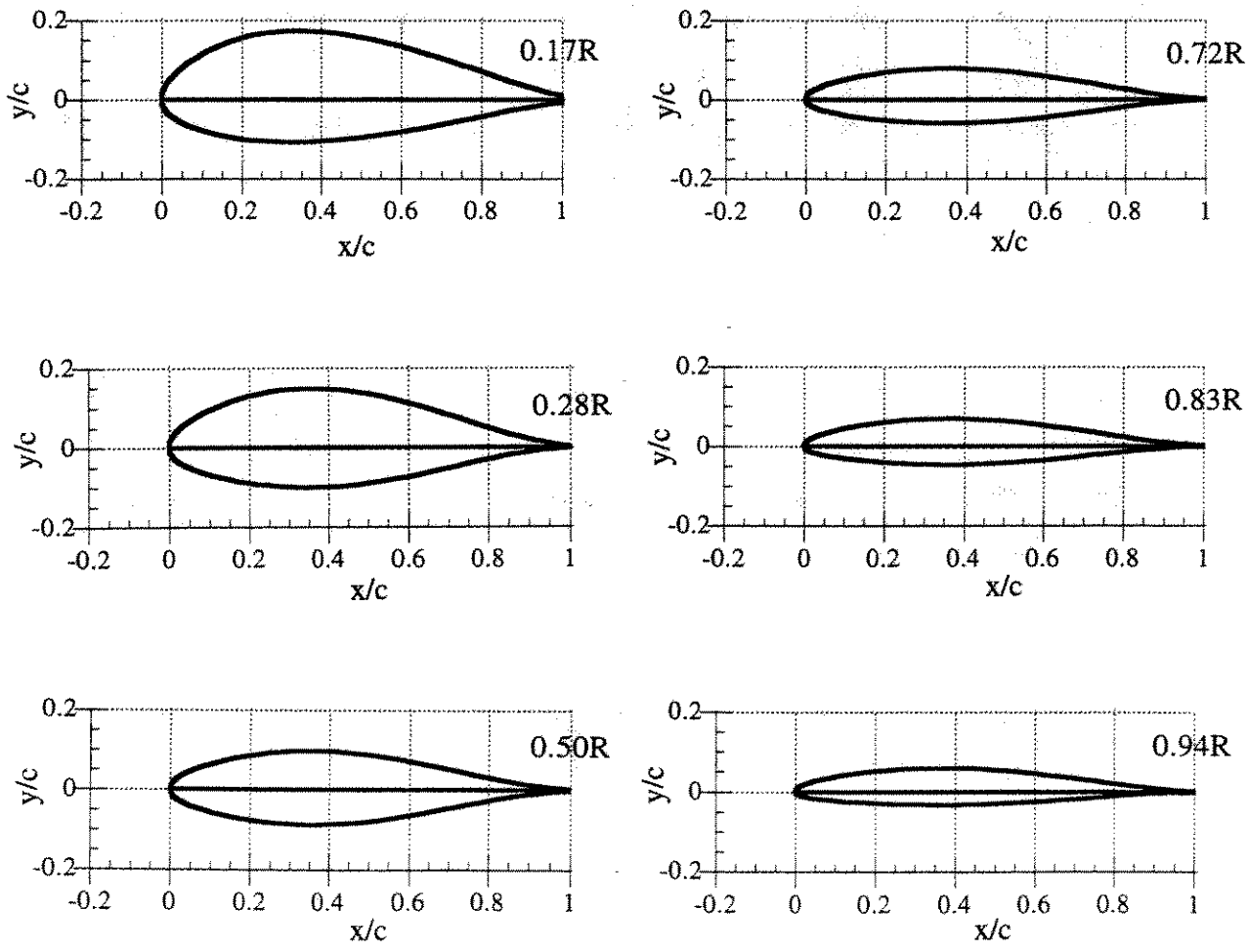

Figure 3(c). Airfoil sections at radial stations of oil-film application.

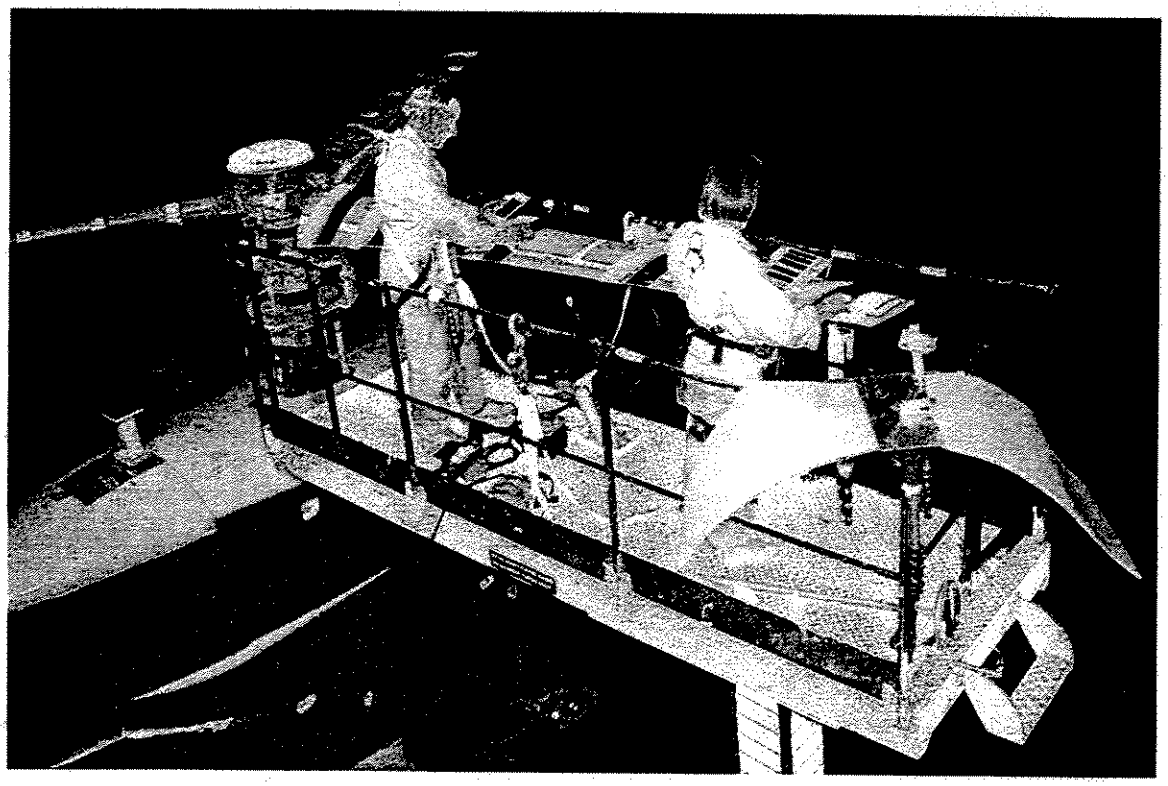

Figure 4. Pre-run oil application.

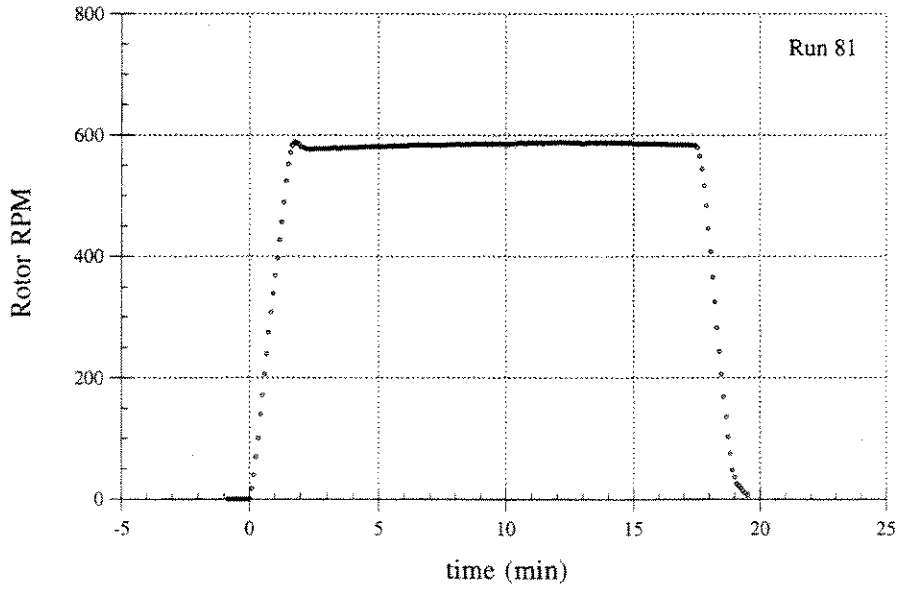

Figure 5. Typical rotor rpm time history.

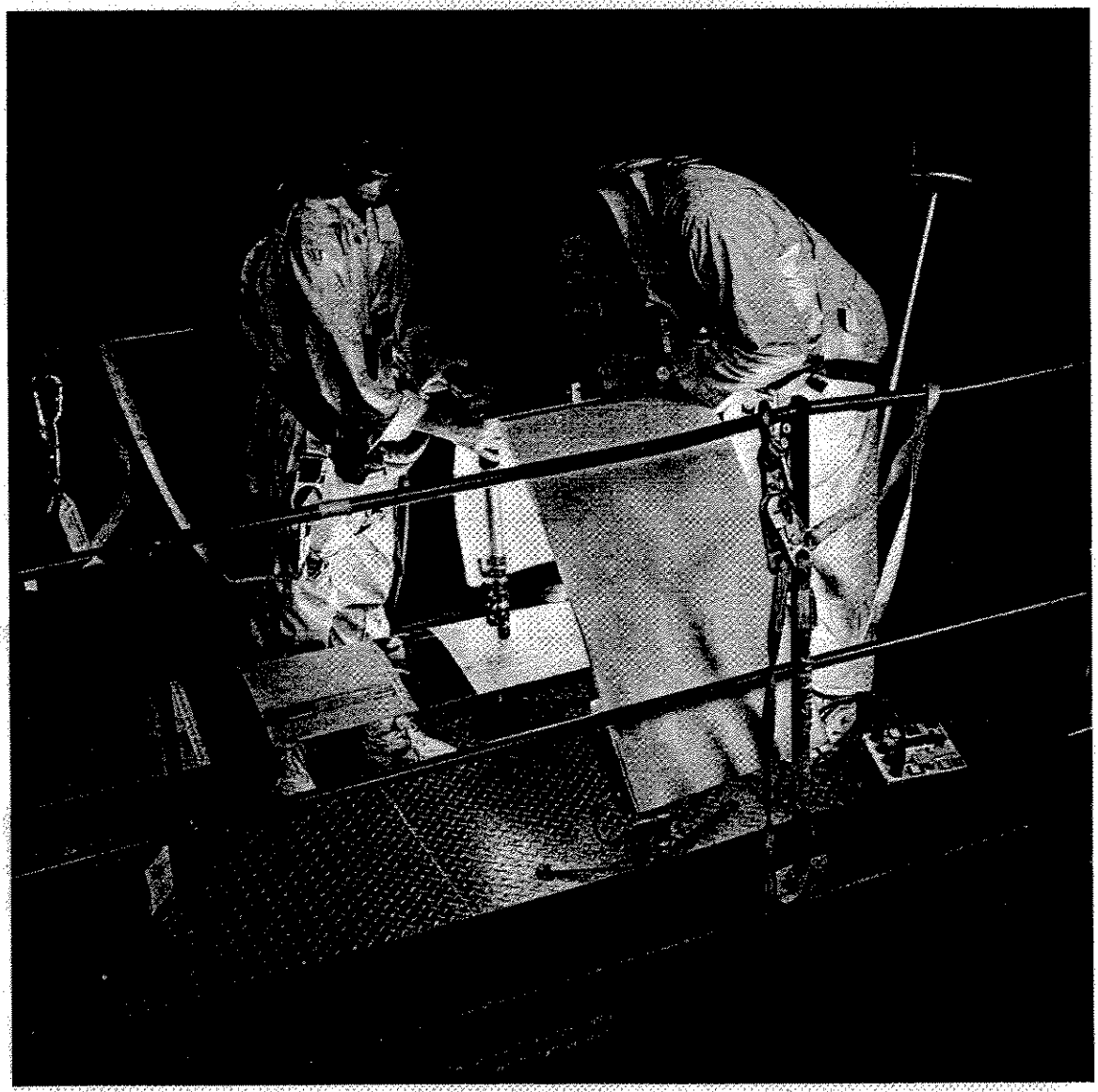

Figure 6. Post-run oil pattern photography.

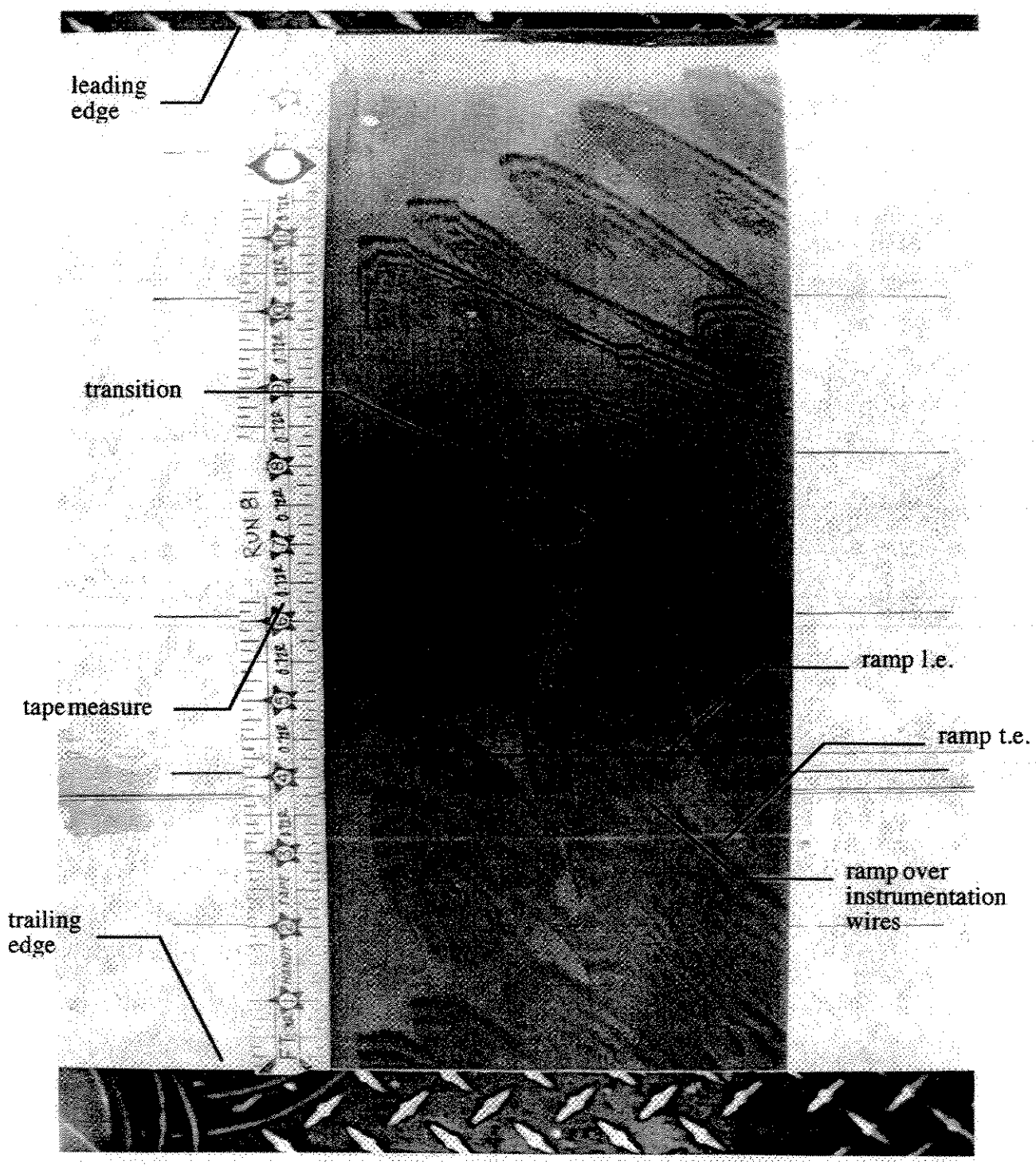

Figure 7. Fringe patterns at r = 0.72R for low thrust condition (Θ = 3 deg).

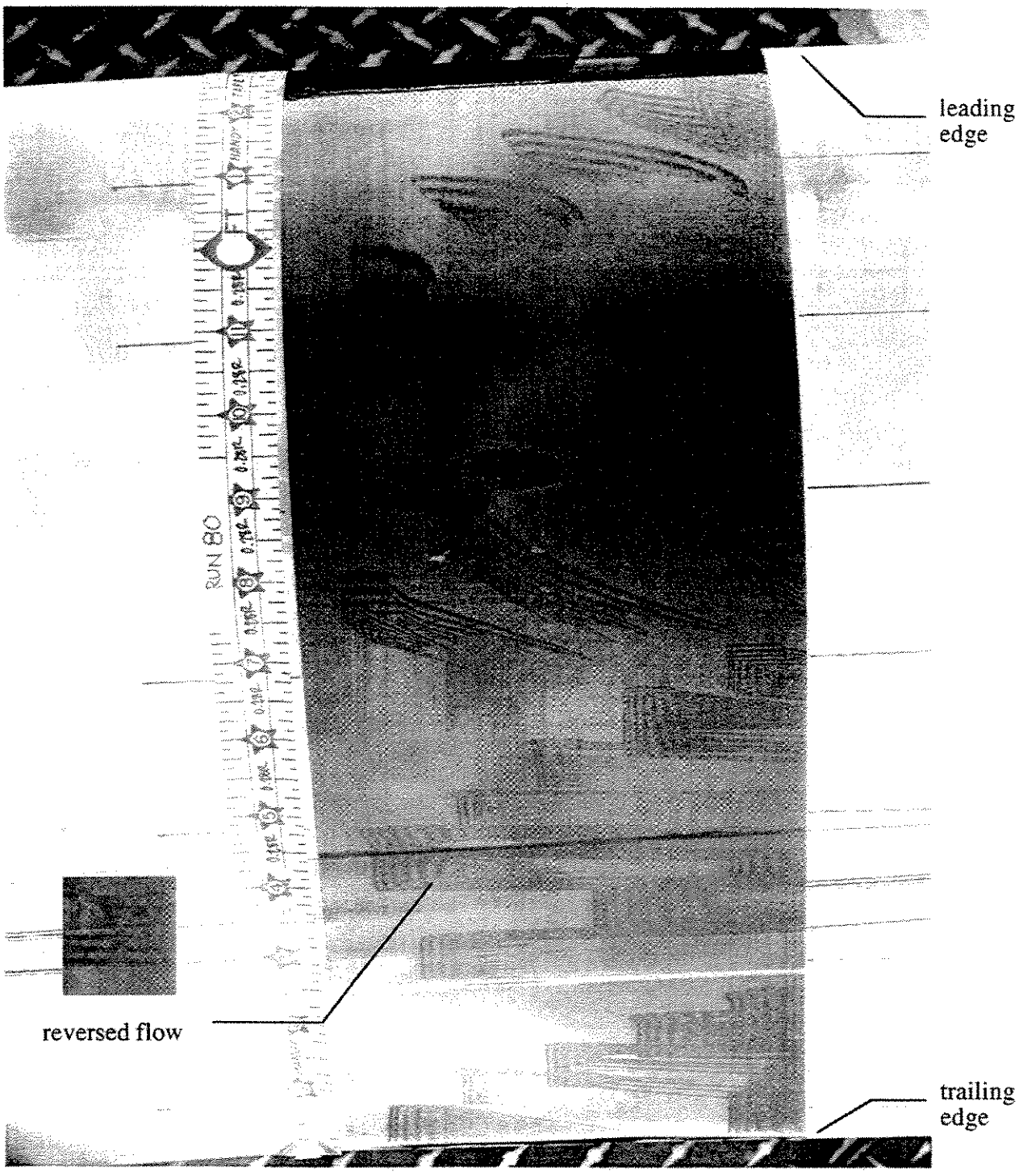

Figure 8. Fringe patterns at r = 0.28R for 1-g hover condition (Θ = 10 deg).

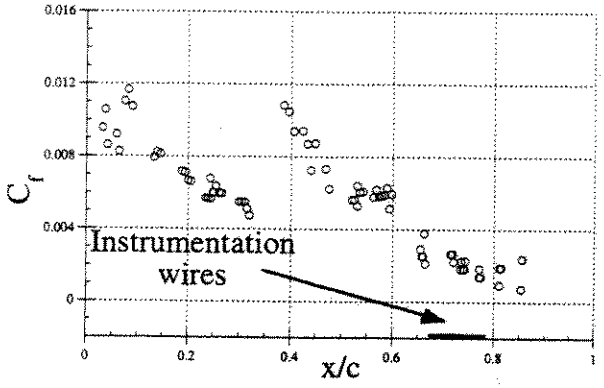

(a) r/R = 0.17

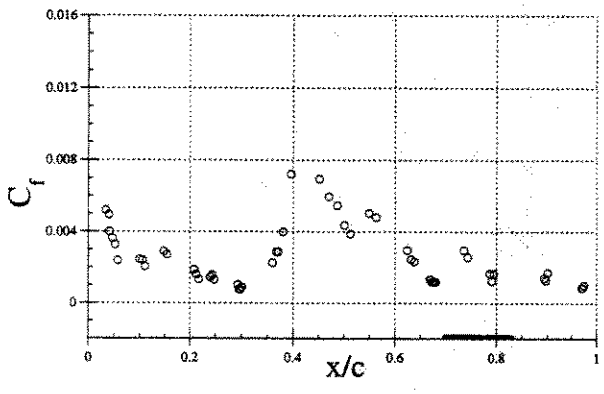

(b) r/R = 0.28

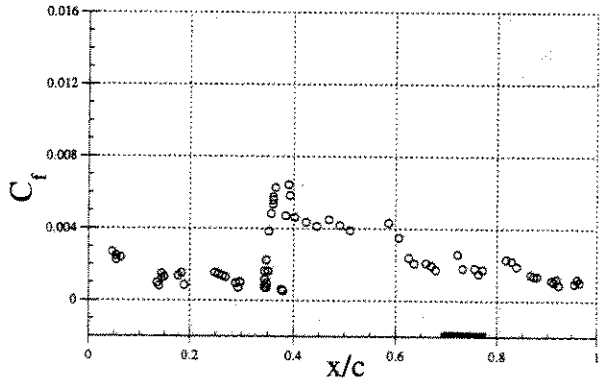

(c) r/R = 0.50

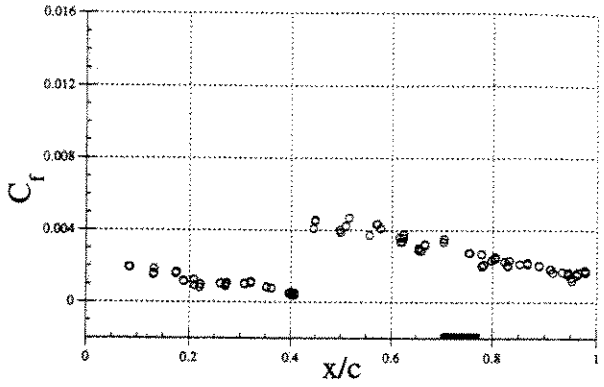

(d) r/R = 0.72

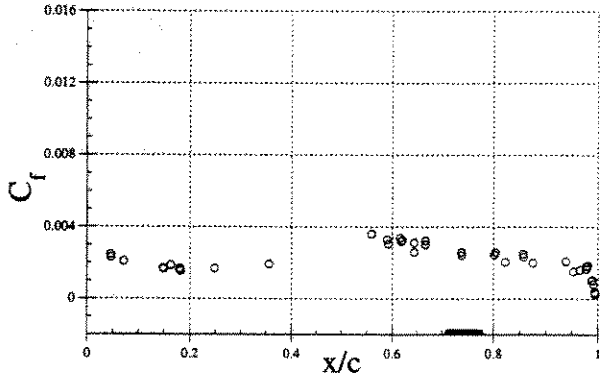

(e) r/R = 0.83

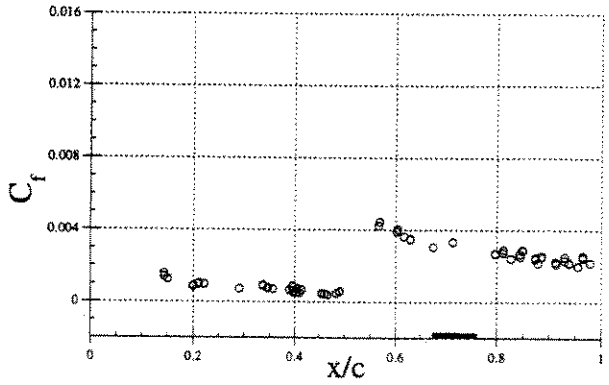

(f) r/R = 0.94

Figure 9. Skin friction distribution at 3 deg collective pitch.

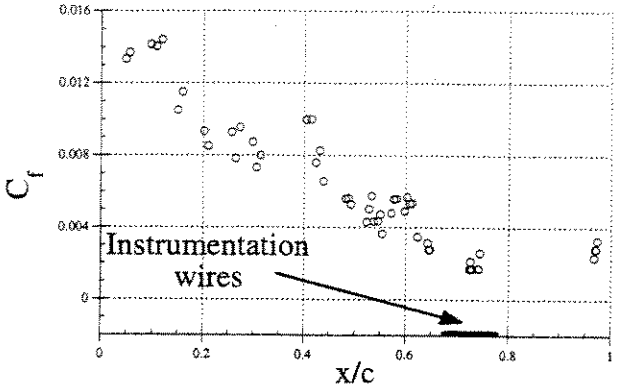

(a) r/R = 0.17

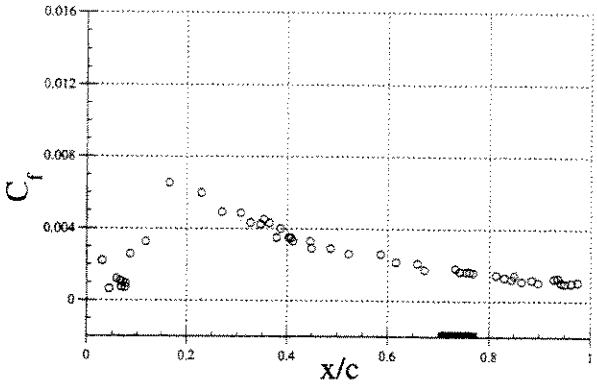

(d) r/R = 0.72

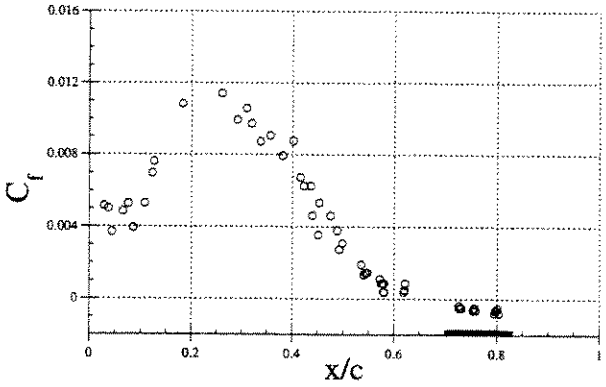

(b) r/R = 0.28

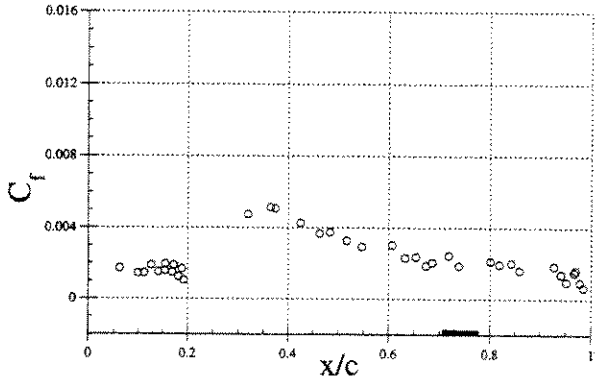

(e) r/R = 0.83

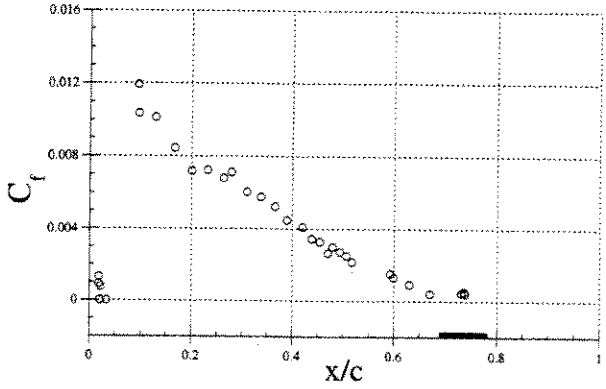

(c) r/R = 0.50

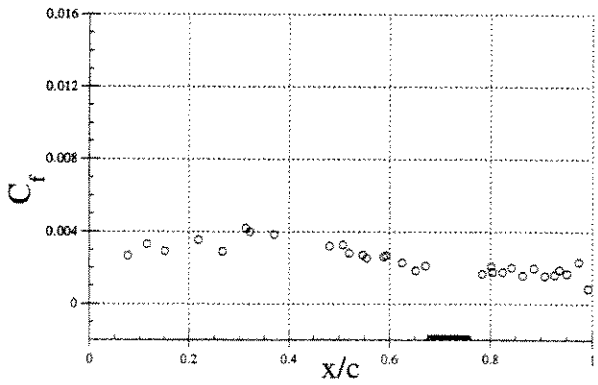

(f) r/R = 0.94

Figure 10. Skin friction distribution at 10 deg collective pitch.

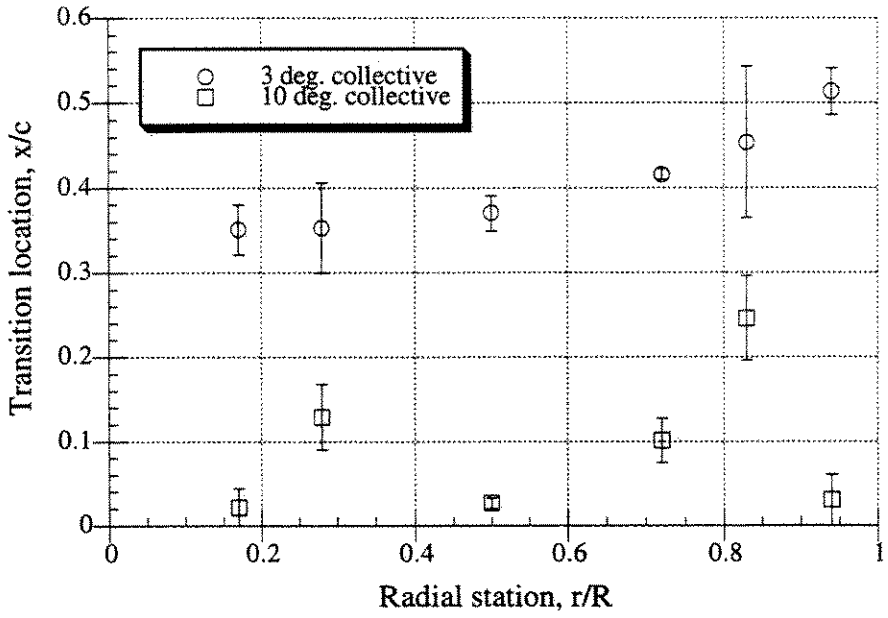

Figure 11. Transition distribution at low and high thrust.